Skin Research and Technology 2013; **19**: e305–e311
Printed in Singapore · All rights reserved
doi: 10.1111/j.1600-0846.2012.00644.x

Skin Research and Technology

Lesion classification using 3D skin surface tilt orientation

Zhishun She[1,2] and P. S. Excell[1,2]

[1]*Institute of Arts, Science & Technology, Glyndwr University, Wrexham, UK, and* [2]*University of Wales, Cardiff, UK*

Background/purpose: Current non-invasive diagnostic procedures to detect skin cancer rely on two-dimensional (2D) views of the skin surface. For example, the most commonly-used ABCD features are extracted from the 2D images of skin lesion. However, because the skin surface is an object in three-dimensional (3D) space, valuable additional information can be obtained from a perspective of 3D skin objects. The aim of this work is to discover the new diagnostic features by considering 3D views of skin artefacts.

Methods: A surface tilt orientation parameter was proposed to quantify the skin and the lesion in 3D space. The skin pattern was first extracted from simply captured white light optical clinical (WLC) skin images by high-pass filtering. Then the directions of the projected skin lines were determined by skin pattern analysis. Next the surface tilt orientations of skin and lesion were estimated using the shape from texture technique. Finally the difference of tilt orientation in the lesion and normal skin areas, combined with the ABCD features, was used as a lesion classifier.

Results: The proposed method was validated by processing a set of images of malignant melanoma and benign naevi. The scatter plot of classification using the feature of surface tilt orientation alone showed the potential of the new 3D feature, enclosing an area of 0.78 under the ROC curve. The scatter plot of classification, combining the new feature with the ABCD features by use of Principal Component Analysis (PCA), demonstrated an excellent separation of benign and malignant lesions. An ROC plot for this case enclosed an area of 0.85. Compared with the ABCD analysis where the area under the ROC curve was 0.65, it indicated that the surface tilt orientation (3D information) was able to enhance the classification results significantly.

Conclusions: The initial classification results show that the surface tilt orientation has a potential to increase lesion classifier accuracy. Combined with the ABCD features, it is very promising to distinguish malignant melanoma from benign lesions.

Key words: 3D skin – tilt orientation – lesion classification – skin lines – melanoma

Accepted for publication 26 April 2012

MALIGNANT MELANOMA is the most fatal type of skin cancer. As detection of malignant melanoma at an early stage considerably reduces its morbidity and patients' mortality, computer automatic diagnosis (CAD) of skin lesions using early symptoms would be particularly useful as an aid in primary care. In order to implement this, a feature set enabling accurate differentiation between benign and malignant skin lesions is required. Most commonly used image-based diagnostic features are related to shape, boundary irregularity, colour variegation and size of skin lesion: the so-called ABCD features (1). These features are extracted from two-dimensional (2D) images of skin, but because the skin surface is an object in three-dimensional (3D) space, valuable additional information can be gained by investigating new features, which are derived from a consideration of 3D skin objects.

Research on acquisition of 3D data and 3D image analysis of skin lesions and wounds has been reported. In 1984, Dhawan et al. (2) captured three images to conduct 3D tomographic imaging. The vertical cross sections of the lesions were calculated to measure their thickness. In 1995, Jones and Plassmann (3) built an instrument based on the principle of colour-coded structured light. A set of parallel stripes was projected on a skin wound and a depth map was deduced from the distortions of the projected stripes. In 2009, Treuillet et al. (4) made use of two images to build 3D models of skin wounds using a structure from motion (SFM) algorithm. However, the computational cost of these methods is high for multiple image calibration and 3D image reconstruction. Recently, the photometric stereo method has been used to detect skin cancer. More than two images are acquired from different illumination

directions (5). The multiple images are combined to recover the reflectance image (6) and the surface normal (7–13). Then the surface normal is used to derive the slant pattern and the tilt pattern. In computer vision, it is a technique of shape from shading. However, in practice the multiple images are not registered precisely, resulting in the errors in the slant pattern and the tilt pattern.

An alternative approach to estimate 3D surface information is the shape from texture technique (14). As most areas of the human skin surface are covered with a network of skin lines (glyphic pattern) (15), the projections of skin lines in the 2D imaging plane are important cues for shape perception in human vision (16). Witkin (17) derived the maximum likelihood (ML) estimator of shape from texture, but it involved a computationally intensive optimization. Garding (18) developed a closed-form solution to extract 3D information. As a single image was employed to estimate the tilt and slant angles, it was simple and efficient.

Shape from texture has been established on homogeneity surface. However, shape from heterogeneous texture is the new research direction and a recent investigation on this topic has been reported (19). The aim of this article is to investigate the potential application of shape from texture technique to detect melanoma. In order to capture the texture of skin surface, the normal White Light Clinic (WLC) images are used (20–22). The work described in this article is to extract 3D information of skin lesions using the surface tilt orientation. The 2D texture was represented by statistical skin line direction. The surface tilts for lesion and skin areas were determined using the shape from texture technique. The disruption of surface tilt in a lesion area was then chosen for lesion classification.

In '3D skin surface orientation', 3D skin surface orientations are defined and are determined by the shape from texture technique. The section'Skin pattern and skin line direction' discusses the skin pattern and analyses the skin line directions with clinical examples. A computational algorithm to extract the feature of surface tilt orientation is described in 'Feature extraction'. The section 'Classification results' conducts lesion classifications and conclusions are drawn in the final section.

3D Skin Surface Orientation

In the theory of shape from texture (14), 3D skin surface orientation is usually represented by the tilt angle and the slant angle, as shown in Fig. 1. Let **n** be the surface normal at point P. The tilt, τ, is the angle between the x-axis of the camera frame, xyz, and the projection of the normal on the image plane, **N**; $\tau\varepsilon[0, 2\pi]$. The slant, σ, is the projected angle of **n** on the $-z$-axis of the camera frame; $\sigma\varepsilon[0, \pi]$.

It is assumed that the skin surface image contains K skin lines. They are distributed uniformly on the 3D skin surface. Let α_k, ($k = 1, \ldots, K$), be the angle between the projected skin line and the x-axis. An auxiliary vector, $[\cos 2\alpha_k, \sin 2\alpha_k]^T$ is introduced: the centre of mass for the projected skin surface is then determined by

$$C = \frac{1}{K}\sum_{k=1}^{K} cos2\alpha_k \tag{1}$$

$$S = \frac{1}{K}\sum_{k=1}^{K} sin2\alpha_k \tag{2}$$

The polar coordinates of the centre of mass are

$$Q = \sqrt{C^2 + S^2} \tag{3}$$

$$\psi = \frac{1}{2} arctan\frac{S}{C} \tag{4}$$

The slant and the tilt are determined by (18)

$$\sigma = arccos\frac{1-Q}{1+Q} \tag{5}$$

$$\tau = \psi \pm \frac{\pi}{2}(mod\, 2\pi) \tag{6}$$

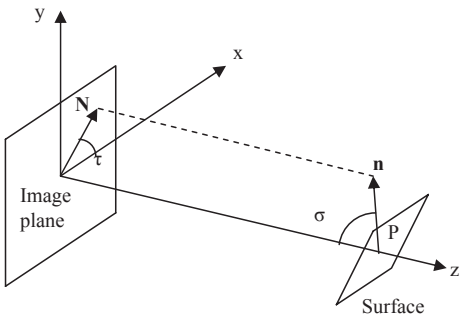

Fig. 1. 3D imaging geometry.

Skin Pattern and Skin Line Direction

In order to calculate the 3D skin surface orientation, the directions of the projected skin lines need to be determined. As the skin lines are only subtly displayed in raw optical skin images, skin pattern analysis is conducted to extract skin lines and estimate their directions. Skin pattern can be produced by high-pass filtering (23). Firstly the skin image is smoothed by convolving with a 9×9 window with a value of 1/81 and then this smoothed image is subtracted from the original. The result is further enhanced by histogram equalization and finally the output is inverted so that the skin lines are seen as high-intensity features.

From a skin pattern image $G(m, n)$, the gradient vector $\nabla G(m, n) = [G_x(m, n), G_y(m, n)]^T$ is calculated, where $G_x(m, n)$ and $G_y(m, n)$ are the gradients in horizontal and vertical directions, respectively. Then, in order to find the skin pattern structure, a local tensor $J(m, n)$ is introduced, that is,

$$J(m,n) = \nabla G(m,n)\nabla G^T(m,n) \tag{7}$$

For a local sub-image with a size of $M \times N$ pixels, the averaged tensor is defined as

$$J = \frac{1}{MN}\sum_{m=1}^{M}\sum_{n=1}^{N} J(m,n) \tag{8}$$

It can be verified that J is positive semi-definite and its eigenvalues are not negative. These eigenvalues reflect the variation of image grey values. The eigenvector corresponding to the smallest eigenvalue is the direction along the skin line where the variation of grey value is least.

J is a 2×2 matrix:

$$J = \begin{bmatrix} f_{xx} & f_{xy} \\ f_{xy} & f_{yy} \end{bmatrix} \tag{9}$$

where

$$\begin{aligned} f_{xx} &= \frac{1}{MN}\sum_{m=1}^{M}\sum_{n=1}^{N} G_x^2(m,n), f_{yy} \\ &= \frac{1}{MN}\sum_{m=1}^{M}\sum_{n=1}^{N} G_y^2(m,n) \ and \\ f_{xy} &= \frac{1}{MN}\sum_{m=1}^{M}\sum_{n=1}^{N} G_x(m,n)G_y(m,n). \end{aligned}$$

The skin line direction is aligned with the angle of the eigenvector corresponding to the minimum eigenvalue, which is (24)

$$\alpha = \frac{1}{2} tan^{-1}\left(\frac{2f_{xy}}{f_{xx} - f_{yy}}\right) \tag{10}$$

Figure 2 shows, from left to right, the original image, skin pattern and skin line directions with lesion boundary. From top to bottom, the first two rows of images are of benign naevi. The latter two rows of images are of malignant melanomas. Skin pattern direction was calculated over a local patch of 16×16 pixels. This size is chosen so that patch data adequately represent the qualities of the major skin pattern and is small enough so that the properties are substantially invariant over each patch. It indicates the disruption of skin line directions by malignant melanomas in comparison with benign naevi.

Feature Extraction

The lesion boundary is determined by a snake-based edge detection technique (25), which makes use of image grey value. The detected boundary segments the image into skin area A_S and lesion area A_l. The surface tilt orientations in the skin and lesion areas are calculated by

$$\tau_s = \frac{1}{2} arctan \frac{\sum\limits_{(i,j)} sin2\alpha(i,j)}{\sum\limits_{(i,j)} cos2\alpha(i,j)} \pm \frac{\pi}{2}\ (mod 2\pi) \quad \forall (i,j) \epsilon A_s \tag{11}$$

and

$$\tau_l = \frac{1}{2} arctan \frac{\sum\limits_{(i,j)} sin2\alpha(i,j)}{\sum\limits_{(i,j)} cos2\alpha(i,j)} \pm \frac{\pi}{2}\ (mod 2\pi) \quad \forall (i,j) \epsilon A_l \tag{12}$$

respectively.

The skin surface tilt orientation represents the 3D shape of the observed skin surface, and the distortion of the lesion surface should be apparent from the change of surface tilt orientation. We therefore take the difference of the surface tilt orientations in the skin and lesion areas as a straightforward measure of 3D shape distortion produced by the lesion. Table 1 shows the sur-

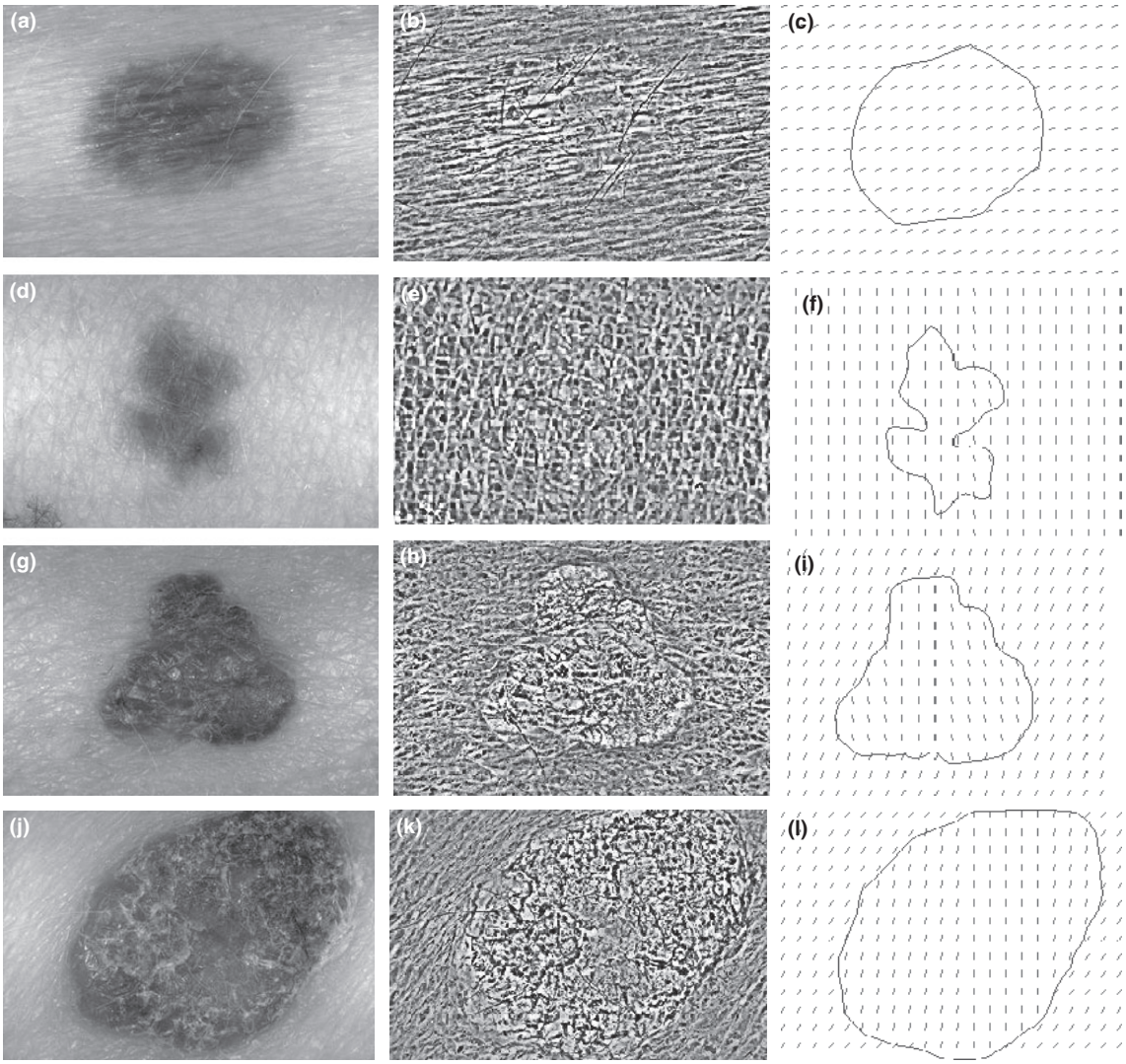

Fig. 2. Left to right: original, skin pattern and skin line directions with lesion boundary. Top to bottom: two examples of benign naevi and two examples of malignant melanoma.

face tilt orientations over skin and lesion areas and their differences for the four examples of skin lesion as shown in Fig. 2, suggesting that the difference in skin surface tilt orientation between skin and lesion might well be a useful classifier.

In summary, the feature extraction of tilt orientation includes four steps: Firstly, skin pattern is produced using high-pass filtering; Secondly, the directions of skin lines on skin surface are determined by Eq. (10); Thirdly, the skin and lesion areas are generated by snake-based edge detection technique; Finally, the tilt orientations of skin and lesions are calculated using Eqs (11) and (12). The difference of tilt orientation is used for lesion classification.

TABLE 1. Surface tilt orientation in skin and lesion areas and their difference in radians

	τ_l	τ_s	$\lvert\tau_l - \tau_s\rvert$
Benign 1	0.8740	0.5658	0.3082
Benign 2	3.3661	3.1561	0.2100
Malignant 1	3.4511	1.5514	1.8998
Malignant 2	2.8273	1.6885	1.1388

Classification Results

The image set used in the experiment of this technique contains examples of several types of lesion, including 26 melanomas and 69 compound or junctional naevi. The melanomas are of various types, sizes and stages of development and the naevi include dysplastic and atypical examples. The total number of cases to be acquired is limited by recruitment of patient

volunteers in clinical practice. The original images were in 24-bit full colour digital format. The resolution of the images is 230 × 350 pixels and the pixel size is 0.04 mm × 0.04 mm. They are chosen to have a reasonable amount of skin area surrounding the lesions.

For lesion classification it is important to determine the sample size. It needs to satisfy $Q > 3cp$ (26), where Q is the sample size, c the number of classes and p the number of features. In this study we have two classes (benign naevi and malignant melanoma) and thus up to three features will be used for lesion classification in order to meet this requirement.

The surface tilt orientations for skin and lesion areas and their differences were calculated: the distribution of the skin surface tilt differences is shown in Fig. 3(a). As expected, there is a tendency to a greater surface tilt orientation deviation in the malignant melanoma images compared to that in the benign lesion images. The receiver operating characteristic (ROC) curve is a plot of the true positive rate against the false positive rate for the different possible cut-off points of a diagnostic test (27). It is commonly used to measure the accuracy of melanoma's diagnosis. Figure 3(b) shows the ROC curve. The area under the curve is greater than 0.78 leading to the conclusion that this could be a useful addition to a diagnostic feature set. Youden index is defined by the summation of sensitivity and specificity -1 and the optimal cut-off point on an ROC curve is the point which has a maximum Youden index (28). The optimal cut-off point in Fig. 3(b) is A. It has a sensitivity of 81% and a specificity of 62%.

The feature of surface tilt orientation was combined with the objective measurements of ABCD features (29–31) to enhance the classification accuracy. Principal component analysis (PCA) was used for this combination. This includes four steps:

(1) For each skin lesion a feature vector is formed by the seven features, surface tilt orientation, asymmetry, border irregularity, red component variegation, green component variegation, blue component variegation and diameter of lesion;
(2) A covariance matrix of feature vector is computed by sample averaging;
(3) Eigenvalues and eigenvectors of the covariance matrix are calculated by singular value analysis (SVA) (32), and a transform matrix is constructed from the eigenvectors corresponding to the first, second and third dominant eigenvalues of the covariance matrix;
(4) The dimension of the feature space is reduced from 7 to 3 by multiplying the transform matrix with each feature vector.

This transformation results in three dominant features for each case. These three dominant features are uncorrelated and are the linear combinations of the seven features extracted from surface tilt orientation and ABCD analysis. These three dominant features were chosen for lesion classification.

The scatter plot of the 95 skin lesions on the three-dimensional dominant feature space is given in Fig. 4(a), which demonstrates that malignant lesions usually distribute in the top-right as they have greater disturbances in the space of the three principal features and thus they can be discriminated from benign lesions. A receiver operating characteristic (ROC) curve was plotted: Fig. 4(b) shows the ROC curve where the area under the curve is greater than

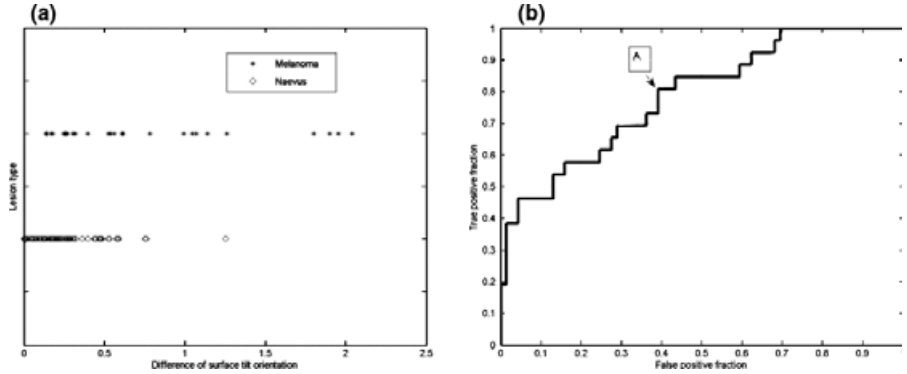

Fig. 3. Lesion classification using surface tilt orientation: (a) Scatter plot of skin lesions and (b) ROC curve for lesion classification.

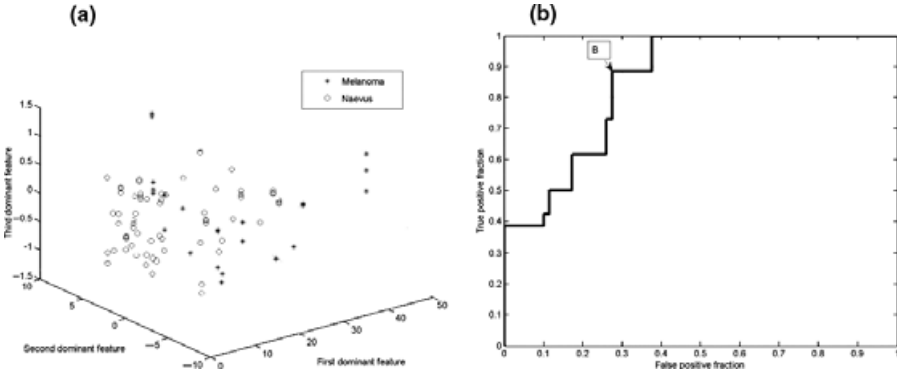

Fig. 4. Lesion classification using combined features: (a) Scatter plot of skin lesions and (b) ROC curve for lesion classification.

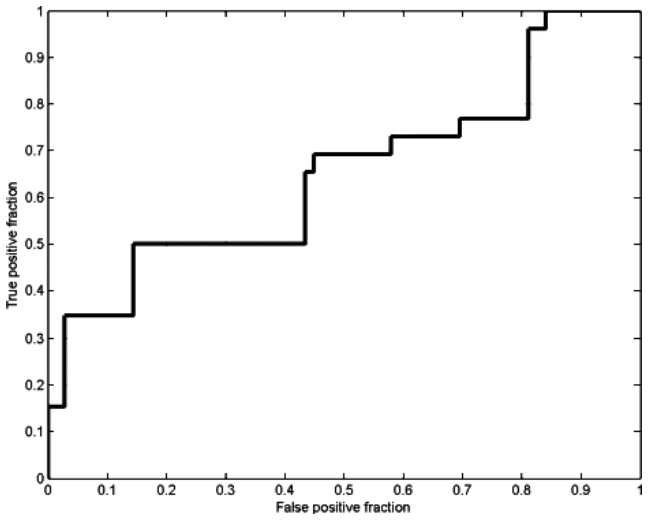

Fig. 5. ROC curve for lesion classification using ABCD analysis.

0.85, indicating an encouraging classification result. The optimal cut-off point B in Fig. 4(b) provides a sensitivity of 89% and a specificity of 72%. Compared with the ROC curve of ABCD analysis shown in Fig. 5 where the area under the ROC curve is 0.65, it shows that the tilt orientation combined with ABCD features is able to improve the classification performance significantly.

The classification test has also conducted by using the training set to set up the classifier and then the test set to assess the classification performance (33). The leave-one-out (LOO) (34) is one of the commonly used methods. It selects a single case from the data set as the test set and the remaining cases as the training set. The classification test is repeated such that each case is used once as the test is set. The classification results are shown in Table 2 which produces a sensitivity of 88%, a specificity of 71% and a classification accuracy of 76%.

TABLE 2. Classification results using LOO

		Actual type	
		MM	BN
	MM	23	20
Classified type	BN	3	49

Conclusions

A new diagnostic feature, tilt orientation, has been developed and suggested as a feature to measure the distortion of 3D skin surface caused by lesions. A 2D image is captured to extract the skin line directions, then skin line directions are employed to estimate tilt orientation using the shape from texture technique. This makes use of one image rather than multiple images and has a small computational load. Classification results comparing tilt orientation in a lesion to that of the surrounding normal skin indicate that the tilt orientation tends to be disrupted by malignant melanoma but not benign naevi, suggesting that this is a promising feature for lesion classification. Combined with the ABCD analysis, the tilt orientation is able to enhance the classification performance.

Acknowledgements

The optical skin lesion images were provided by M Dickson, V Wallace and Dr J Bamber of the Physics Department, Clinical Research Centre, Royal Marsden Hospital, Sutton. Permission to use them is gratefully acknowledged. This work was funded by EPSRC grants GR/M72371 and GR/M72289. Recently it has been supported by a Natural Science Foundation project of CQ CSTC.

References

1. Friedman RJ, Rigel DS, Alfred WK. Early detection of malignant melanoma: the role of physician examination and self-examination of the skin. CA Cancer J Clin 1985; 35: 130–151.
2. Dhawan A, Gordon R, Rangayyan R. Nevoscopy: three-dimensional computed tomography of nevi and melanomas in situ by transillumination. IEEE Trans Med Imaging 1984; 3: 54–61.
3. Jones B, Plassmann P. An instrument to measure the dimensions of skin wounds. IEEE Trans Biomed Eng 1995; 42: 464–470.
4. Treuillet S, Albouy B, Lucas Y. Three-dimensional assessment of skin wounds using a standard digital camera. IEEE Trans Med Imaging 2009; 28: 752–762.
5. Woodham RJ. Photometric method for determining surface orientation from multiple images. Opt Eng 1980; 19: 139–144.
6. Sun J, Smith ML, Smith LN, Coutts L, Dabis R, Harland C, Bamber J. Reflectance of human skin using colour photometric stereo - with particular application to pigmented lesion analysis. Skin Res Technol 2008; 14: 173–179.
7. Ding Y, Smith L, Smith M, Sun J, Warr R. Obtaining malignant melanoma indicators through statistical analysis of 3D skin surface disruptions. Skin Res Technol 2009; 15: 262–270.
8. Ding Y, Smith L, Smith M, Warr R. 3D skin texture analysis for early diagnosis of malignant melanoma. *Proceedings of Medical Image Understanding and Analysis*, Aberystwyth, UK, July 2007, 151–155.
9. Ding Y, Smith L, Smith M, Warr R, Sun J. Obtaining 3D malignant melanoma indicators through the analysis of skin tilt pattern and skin slant pattern. *Proceedings of MICCAI workshop on Microscopic Image Analysis with Application to Biology (MIAAB)*, New York, USA, September 2008, 64–71.
10. Ding Y, Smith L, Smith M, Warr R, Sun J. Enhancement of skin tilt pattern for lesion classification. *Proceedings of IASTED international conference on visualization, imaging and image processing*, Palma de Mallorca, Spain, September 2008, 1–6.
11. Zhou Y, Smith M, Smith L, Warr R. Using 3D differential forms to characterize a pigmented lesion in vivo. Skin Res Technol 2010; 16: 77–84.
12. Zhou Y, Smith M, Smith L, Farooq A, Warr R. Enhanced 3D curvature pattern and melanoma diagnosis. Comput Med Imaging Graphics 2011; 35: 155–165.
13. Ding Y, Smith L, Smith M, Sun J, Warr R. A computer assisted diagnosis system for malignant melanoma using 3D skin surface texture features and artificial neural network. Int J Model Ident Control 2010; 90: 370–381.
14. Trucco E, Verri A. Introductory techniques for 3D computer vision. Englewood Cliffs, NJ: Prentice-Hall, Inc., 1998.
15. Wilhelm K, Elsnor P, Berardesca E. Bioengineering of the skin: skin surface imaging and analysis. Boca Raton, FL: CRC press, Inc.; 1997.
16. Gibson J. The perception of the visual world. Boston, MA: Houghton Mifflin; 1950.
17. Witkin AP. Recovering shape and orientation from texture. Artif Intell 1981; 17: 17–45.
18. Garding J. Direct estimation of shape from texture. IEEE Trans Pattern Anal Mach Intell 1993; 15: 1202–1207.
19. Loh AM, Hartley R. Shape from nonhomogeneous, nonstationary, anisotropic, perspective texture. *Proceedings of the British Machine Vision Conference*, Oxford, UK, September 2005, 1–10.
20. Cottrell WJ, Oseroff AR, Foster TH. Portable instrument that integrates irradiation with fluorescence and reflectance spectroscopies during clinical photodynamic therapy of cutaneous disease. Rev Sci Instrum 2006; 77: 1–8.
21. Prince S, Malarvizhi S, SreeHarsha KCA, Bhandari A, Dua A. An automated system for optical imaging to characterize tissue based on diffuse reflectance spectroscopy. *Proceedings of the Biomedical Robotics and Biomechatronics (BioRob) Conference*, Scottsdale, AZ, USA, October 2008, 736–739.
22. Prince S, Malarvizhi S, SreeHarsha KCA, Bhandari A, Dua A. A non-invasive diffuse reflectance optical spectroscopic imaging system to characterize tissue. *Proceedings of the IEEE International Conference on Automation and Logistics*, Hong Kong and Macau, China, August 2008, 77–80.
23. Round AJ, Duller AWG, Fish PJ. Lesion classification using skin patterning. Skin Res Technol 2000; 6: 183–192.
24. She Z, Fish P. Analysis of skin line pattern for lesion classification. Skin ResTechnol 2003; 9: 73–80.
25. She Z, Fish PJ. Boundary detection of skin lesion using a fast snake algorithm. *Proceedings of 16th Biennial International EURASIP Conference*, Brno, Czech Republic, June 2002, 295–297.
26. Foley DH. Consideration of Sample and Feature Size. IEEE Trans Inf Theory 1972; 18: 618–626.
27. Swets JA, Dawes RM, Monahan J. Better decisions through science. Sci Am 2000; 283: 70–75.
28. Schisterman EF, Perkins NJ, Liu A, Bondell H. Optimal cut-point and its corresponding Youden index to discriminate individuals using pooled blood samples. Epidemiology 2005; 16: 73–81.
29. She Z, Liu Y, Damatoa A. Combination of features from skin pattern and ABCD Analysis for lesion classification. Skin Res Technol 2007; 13: 25–33.
30. Ercal F, Chawla A, Stoecker WV, Lee HC, Moss RH. Neural network diagnosis of malignant melanoma form colour images. IEEE Trans Biomed Eng 1994; 41: 837–844.
31. Ganster H, Pinz P, Rohrer R, Wildling E, Binder M, Kittler H. Automated melanoma recognition. IEEE Trans Med Imaging 2001; 20: 233–239.
32. Golub GH, Loan CFV. Matrix computations. Baltimore, MD: Johns Hopkins University Press; 1989.
33. Rosado B, Menzies S, Harbauer A, Pehamberger H, Wolff K, Binder M, Kittler H. Accuracy of Computer Diagnosis of Melanoma - a Quantitative Meta-analysis. Arch Dermatol 2003; 139: 361–367.
34. Theodoridis S, Koutroumbas K. Pattern recognition. San Diego, CA: Academic Press; 2003.

Address:
Zhishun She
Institute of Arts, Science & Technology
Glyndwr University
Wrexham
UK
Tel: 44 1978 293414
Fax: 44 1978 293168
e-mail: z.she@glyndwr.ac.uk